A direct ethylene glycol fuel cell stack as air-independent power sources for underwater and outer space applications

Zhefei Pan[1], Heran Zhuang[1], Yanding Bi, Liang An*

Department of Mechanical Engineering, The Hong Kong Polytechnic University, Hung Hom, Kowloon, Hong Kong SAR, China.

[1] Equal contribution.

*Corresponding author.

Email: liang.an@polyu.edu.hk (L. An)

Abstract

A passive direct ethylene glycol fuel cell stack is developed and tested, in which each single cell consists of an alkaline Pd-based anode, an acid Au-based cathode, and a cation exchange membrane. This passive stack design eliminates the gas blowers/compressors for the air supply, external liquid pumps for the liquid fuel supply, or any other auxiliary devices. Hence, the passive design reduces both volume and weight of the stack comparing to the active fuel cell stack, thus both volumetric energy density and specific energy density are much improved. In this study, an alkalized ethylene glycol aqueous solution is used as fuel and an acidified hydrogen peroxide aqueous solution is used as oxidant, respectively. As a result, the theoretical voltage of this fuel cell stack is increased from 2.18 V to 4.94 V comparing to the design using the air, which shows a promising potential for practical applications. Experimentally, at the optimal reactant-feeding concentrations of 5.0 M EG and 9.0 M KOH as anolyte and 4.0 M H_2O_2 and 1.0 M H_2SO_4 as catholyte, this passive stack yields an open-circuit voltage of 3.0 V, a maximum current of 860 mA, and a peak power of 1178 mW at room temperature, which exhibits a two-time higher peak power density (24.5 mW cm^{-2}) than a passive stack using the same type of fuel but the air as oxidant (12 mW cm^{-2}). The impressive improvement can be

ascribed to the faster hydrogen peroxide reduction reaction due to its two-electron transfer process rather than a four-electron process. In addition, the effects of feeding concentrations in both anolyte and catholyte on the stack performance are studied. Finally, the present passive stack is applied to power an electric fan for around 3 hours under the mimetic underwater circumstance, demonstrating that this passive stack is a promising power source for airtight situations, such as underwater and outer space.

Keywords: Direct ethylene glycol fuel cells; Passive fuel cells; Fuel cell stack; Hydrogen peroxide; Feeding concentrations; Underwater operation

1. Introduction

Direct liquid fuel cells (DLFCs) that use liquid alcohols as fuel, e.g. methanol, ethanol, and ethylene glycol (EG), to replace gaseous hydrogen have been regarded as one of the most promising power generation technologies for portable electronics [1-5]. In spite of the general superiorities of fuel cells, such as simple design, high energy conversion efficiency, low emissions as well as quick refueling [4, 6], the DLFCs exhibits a broader range of advantages including mature production, easy transportation, and convenient handling of liquid fuels comparing to hydrogen fuel cells [7-11]. Among various liquid fuels, EG has received considerable interests because of the electron transfer rate as high as 80%, the boiling point of 198ºC, and the theoretical energy capacity of 4.8 Ah mL^{-1}, which is a promising fuel for electronic devices [12, 13]. In addition, the toxicity of EG is low and it can be produced by hydration of ethylene oxide (EO) efficiently [14]. Therefore, direct ethylene glycol fuel cells (DEGFCs) have attracted ever-increasing attention, particularly these fuel cells using anion exchange membranes (AEMs) due to the both enhanced anodic and cathodic kinetics [15-18]. AEMs and cation exchange membranes (CEMs) are classified by the charge type of fixed functional groups, which can selectively allow the passage of oppositely charged ions (counter-ions), while obstruct similarly charged ions (co-ions) [19]. An et al. [20] compared the AEM and CEM in direct ethanol fuel cells (DEFCs). It was found that the AEM possessed the higher ionic conductivity and mechanical property, but the worse thermal stability. In addition, the CEM showed the lower ionic conductivity, but acceptable thermal stability, mechanical property, and species permeability. There is no significant difference in the fuel cell performance between the AEM and CEM at low operating temperatures (<60ºC), but the CEM-DEFC can operate stably at high operating temperatures (typically 90ºC).

In the past decade, numerous effects have been made on performance improvement, catalyst development, and system innovations [21-28]. An et al. [21] developed and tested an alkaline

DEGFC using an AEM, which exhibited a peak power density of 67 mW cm^{-2} at 60ºC. The outstanding performance was ascribed to the alkaline environment, which much enhances the kinetics of both the oxygen reduction reaction (ORR) and ethylene glycol oxidation reaction (EGOR). Considering the poor stability of AEM at high temperatures, generally over 60ºC, they replaced the AEM with an alkali-doped polybenzimidazole in an alkaline DEGFC, which allows the operation of the fuel cell at higher temperatures (90ºC). As a result, it was found that a higher peak power density of 112 mW cm^{-2} was achieved at 90ºC [22]. To improve the activity of the catalyst toward EGOR, Feng et al. [23] reported networked Pt-Pb nanowires (NWs), which was synthesized via a large-scalable wet-chemical approach. The electrocatalyst showed a 3D networked structure with rich defects/steps. To further promote the cell performance and extend the application situations to underwater and outer space, Pan et al. [29] reported that an open-circuit voltage (OCV) of 1.41 V and a peak power density of 80.9 mW cm^{-2} at 60ºC were achieved by replacing the oxygen with hydrogen peroxide in the DEGFC. This type of DEGFC boosted the OCV by 62.1% and the peak power density by 20.8%, as well as eliminated the requirement of air from the ambient environment. Using the acidified hydrogen peroxide rather than the oxygen or air in the cathode as the oxidant has been tested in fuel cells running on various fuels such as formate [30], propanol, and glycerol [31]. Li [30] found that the AEM direct formate-peroxide fuel cell showed a more stable cell voltage than the AEM direct ethanol fuel cell in a conceptual half-hour constant-current discharge. Chino et al. [31] reported that the split pH environment improved the thermodynamics of the fuel cell by creating a large potential difference between electrodes. However, the decomposition of H_2O_2 and thus generation of O_2 may form a two-phase flow in the cathode flow channel, resulting in the voltage fluctuation, which is not desirable in the practical applications. Meanwhile, it creates a large transport resistance of H_2O_2 from the cathode flow channel to the

cathode CL, which may lead to the H_2O_2 in the cathode CL at a starving state, thus the cathodic reaction kinetics is sluggish [32].

Moreover, to meet the voltage requirement of electronics in practice, a fuel cell stack rather than a single cell is used, which is constituted by cells connected in series. Cremers et al. [33] developed an active AEM-DEGFC stack using the air as oxidant. When the feeding rates were 12 mL min^{-1} on the anode and 800 sccm on the cathode, the fuel cell stack showed a peak power density of 44 mW cm^{-2} at 50°C. Although the performance is promising, the active operation mode needs auxiliary equipment such as liquid pumps and gas compressors, leading to a more complicated and heavier system [34, 35]. To meet the demand for portable electronic devices, the active operation mode can be replaced by a passive way, which makes the reactants store in the reservoirs and transport to the catalyst layer mainly via diffusion, driven by the concentration gradient [36]. It should be mentioned that the delivery of reactants at the passive operation mode in the porous electrode is slower than the active one does, which is attributed to the fact that an additional driving force of convection for the delivery of reactants exits at the active operation mode. Hence, the passive fuel cell performance is generally lower than the active fuel cell does at the same operation conditions. Pan et al. [37] developed a passive DEGFC with hydrogen peroxide as oxidant. This fuel cell exhibited peak power densities of 30.3 and 65.8 mW cm^{-2} at 23 and 60°C, respectively. Marchionni et al. [38] synthesized Pd-(Ni-Zn)/C catalyst, which was Pd nanoparticles supported on a Ni–Zn phase, and adopted it as the anode catalyst in a passive DEGFC. It was found that the peak power density increased from 12 mW cm^{-2} to 24 mW cm^{-2} at 25°C when the Pd-(Ni-Zn)/C replaced the Pd/C. Fashedemi et al. [39] prepared Pd-based ternary core-shell (FeCo@Fe@Pd) nanocatalyst using multi-walled carbon nanotubes bearing carboxylic (MWCNT-COOH) as supporting platform and compared its performance with the Pd/MWCNT-COOH in a passive DEGFC. It was reported that the running time of the fuel cell using the FeCo@Fe@Pd/MWCNT-COOH-based anode

was around 4.7 h at a discharging current density of 20 mA cm^{-2}, which was higher than the Pd/MWCNT-COOH-based anode did (3.3 h).

In this study, being motivated by the practical needs for reducing the design complexity of the fuel cell system as well as the high voltage requirement of electronics in practice, we designed, fabricated, and tested a passive DEGFC stack, constituted by two single cells, using hydrogen peroxide as oxidant, which avoids the use of liquid pumps and gas compressors as well as possesses a promising theoretical OCV of 4.94 V. As a result of the simpler structure, the specific energy density and volumetric energy density are increased, and the design complexity is reduced significantly. Moreover, the replacement of the oxygen provided from the environment by the hydrogen peroxide in the proposed fuel cell stack is in favor of allowing the fuel cell stack to be air-independent power sources for underwater and outer space applications. Although it is attractive, the H_2O_2 is not stable and will be decomposed to oxygen and water, thus the produced oxygen will reduce the electrochemical surface area (ECSA) and block the channels for reactant delivery, to which future research attention can be paid. The effects of feeding concentrations on the fuel cell stack performance are investigated. When the fuel cell stack is operated at the optimal reactant-feeding concentrations of 5.0 M EG and 9.0 M KOH as anolyte and 4.0 M H_2O_2 and 1.0 M H_2SO_4 as catholyte, it exhibits an actual OCV of 3.0 V, a maximum current of 860 mA, and a peak power of 1178 mW at room temperature. It is found that the whole running time of the fan powered by this passive fuel cell stack was 2 hours and 36 minutes underwater, which was similar to the that in the natural circumstance, demonstrating that this passive fuel cell stack is a promising power source for airtight situations, such as underwater and outer space.

2. Working principle

As depicted in Fig. 1 (a), the passive stack is constituted by two single cells connected in series, which are named as cell 1 and cell 2. The single cell is symmetrically constructed. From the

anode to the cathode, the components are the anode diffusion layer (DL), the anode catalyst layer (CL), the CEM, the cathode CL, and the cathode DL in sequence. In cell 1, the anolyte diffuses from the anode reservoir to the anode CL driven by the concentration gradient, where EGOR occurs and oxalate, electrons and water are produced as shown in Eq. (1) [12]:

$$C_2H_6O_2+10OH^-\rightarrow(COO^-)_2+8e^-+8H_2O \qquad E_{EGOR}=-0.69\ V \qquad (1)$$

The electrons produced by the EGOR of cell 1 are transported from the anode to the cathode of cell 2 through the external circuit. At the same time, H_2O_2 and protons in the cathode reservoir of cell 2 are transported through the cathode DL to the CL and react with coming electrons to produce water, which is known as the hydrogen peroxide reduction reaction (HPRR) [40]:

$$4H_2O_2+8H^++8e^-\rightarrow8H_2O \qquad E_{HPRR}=1.78\ V \qquad (2)$$

Meanwhile, the EGOR occurs in the anode of cell 2 and the electrons produced are transported through the external circuit to the cathode of cell 1. The HPRR is induced in the cathode of cell 1 when receiving the electrons from the anode of cell 2. In both cell 1 and cell 2, the potassium ions transport from the anode to the cathode to complete the internal ionic circuit. The overall reaction is obtained by combining the EGOR and HPRR, which achieves a significantly high theoretical voltage of 2.47 V for a single cell [37]:

$$C_2H_6O_2+4H_2O_2+8H^++10OH^-\rightarrow(COO^-)_2+16H_2O \qquad E=2.47\ V \qquad (3)$$

3. Experiment

3.1. Membrane electrode assembly preparation

The membrane electrode assembly (MEA) is the key component in the passive stack. Two pairs of home-made anodes and cathodes with an active area of 3.0 cm × 8.0 cm are used in the two single cells and the pretreated Nafion 211 (30 μm in the dry state) is selected as the CEM due to the smaller thickness. The Pd-based anode could be fabricated by the method in the open literature [41]. The preparation of the catalyst ink was mixing the ethanol, 5 wt.% Nafion (Fuel

Cell Store, USA), and 30 wt. % Pd/C (Sigma-Aldrich Co., USA). Afterwards, the mixed ink underwent an ultrasonic treatment in the ultrasonic oscillating instrument for 30 minutes. Then the catalyst ink was coated on the carbon cloth (Hesen, China) by a spraying method until the catalyst loading reached 1.0 mg_{Pd} cm^{-2}. Similarly, 60 wt. % Au/C (Premetek Co., USA) was mixed with 15 wt. % Nafion and ethanol to prepare the cathode catalyst ink, which was then sprayed on the carbon cloth by the same method, and the catalyst loading of the catalyst was 2.75 mg_{Au} cm^{-2}. In terms of the preparation of CEMs, the membranes were cut to an area of 4.0 cm × 9.0 cm so that it can fully cover the electrode, which were then immersed in the 2.5 M KOH solution. After one-hour immersion at 80°C, DI water was used to wash the membrane for three times and the membrane was kept in DI water for further assembly.

3.2. Fuel cell setup and instrumentation

As depicted in Fig. 1 (b), the stack consists of two pairs of MEAs, three endplates, four reservoirs, four current collectors, and assorted screws. In case of corrosion by the acid and alkaline environments, 1Cr18Ni9Ti stainless steel and 316L stainless steel were chosen as the materials of endplates and current collectors, respectively. The electrolyte reservoir was designed to be transparent by using polymethyl methacrylate (PMMA) with a hole drilled on the top so that the process of anolyte/catholyte injection is visible. Polytetrafluoroethylene (PTFE) gaskets were added between each layer of the stack to prevent the leakage. The two single cells were connected in series and the electrode arrangement of these two single cells were opposite to avoid the formation of internal fuel cell and self-discharging. The polarization curve and internal resistance of the passive fuel cell stack were tested by using Arbin BT2000 (Arbin instrument Inc.).

4. Results and discussion

4.1. General stack performance

Fig. 2 (a) shows the results of the polarization test and the power of the passive stack at room temperature with 5.0 M EG and 9.0 M KOH as anolyte and 4.0 M H_2O_2 and 1.0 M H_2SO_4 as catholyte. It is demonstrated that the passive stack outputs an OCV of 3.0 V, a maximum current of 860 mA, and a peak power of 1178 mW. In a previous study [42], when EG was used as fuel in the anode and O_2 was used as oxidant in the cathode, the passive single cell achieved an OCV of 0.7 V and a peak power density of 12 mW cm^{-2}. The passive stack in this study exhibits an OCV (3.0 V) four times higher than 0.7 V and a peak power density (24.5 mW cm^{-2}) twice higher than 12 mW cm^{-2}. The performance elevation of this passive stack is mainly ascribed to the superior nature of HPRR comparing to ORR. The two-electron-transfer process of HPRR is more beneficial to the fuel cell performance due to the enhancement of reaction kinetics and a higher theoretical voltage comparing to the four-electron-transfer process of ORR [43]. However, the practical OCV of the stack (3.0 V) is significantly lower than the theoretical OCV (4.94 V). In general, the theoretical OCV can hardly achieve due to the presence of the activation loss, which is caused by the slowness of the reactions taking place on the surface of the electrodes as well as the poor reversibility of anodic and cathodic reactions. Hence, a proportion of the voltage generated is sacrificed to drive the chemical reaction that transfers the electrons to or from the electrode [44]. From this perspective, four methods can be adopted to reduce the activation loss, which are raising the fuel cell operating temperature, using more effective catalysts, increasing the roughness of the electrode, and increasing the reactant concentrations appropriately [45]. In addition, the large OCV loss is associated with the H_2O_2 as well. The H_2O_2 in the cathode is supposed to be used as oxidant, nonetheless, the H_2O_2 also can be oxidized, which establishes of an internal H_2O_2-based fuel cell and causes the mixed potential in the cathode [37]. Moreover, the H_2O_2 is not stable and will be decomposed to oxygen and water. The produced oxygen gas results in two disadvantages. On one hand, the active sites on the catalyst particle may be covered by oxygen,

reducing the electrochemical surface area. On the other hand, oxygen in the porous DL and CL will block the pathways for the reactant transport.

The consistency of the individual cell was investigated by monitoring the voltage of cell 1 and cell 2 at different current densities. As shown in Fig. 2 (b), the voltage of the two cells exhibited a good consistency over the whole current region. However, it can be observed that the voltage of cell 1 decreased slightly faster than cell 2 with increasing current, which was ascribed to the higher internal resistance of cell 1. The good conformance of individual cell consistency reflects a high degree of reproducibility achieved by the appropriate electrode manufacturing process [46], which predicts a promising future for the mass production in practical applications.

Meanwhile, the transient OCV behavior of the stack was investigated. The cell stack was first discharged completely and rested for 20 minutes, and the OCV was recorded and shown in Fig. 3 (a). The OCV of the stack increased rapidly in the first 5 minutes and stabilized at around 2.8 V subsequently. The OCV of this passive stack did not experience a decrease after reaching the maximum value during the rest period, which is different from some other types of fuel cell, such as the direct methanol fuel cells (DMFCs) and DEFCs [47]. This performance improvement is ascribed to the fact that the Au catalyst is inactive to EG, thus the mixed potential problem in the cathode is eliminated, which leads to the stable OCV during the rest period.

Moreover, the constant discharging behavior of this stack was studied. As shown in Fig. 3 (b), when the discharging process was conducted at a constant current of 150 mA, the stack was operated with a stable voltage around 2.5 V for about 160 minutes, presenting a stable and satisfactory performance. In addition, the cost of this passive fuel cell stack can be obtained by summing up the cost of all the components. The unit prices of the anode catalyst, cathode

catalyst, CEM, and DL are \$42.7 g^{-1}, \$136 g^{-1}, \$0.07 cm^{-2}, and \$0.11 cm^{-2}, respectively. Based on the usage of materials in the electrode fabrication, the anode catalyst costs around \$8.59, the cathode catalyst is around \$35.90, the CEMs are about \$4.86, the DLs are about \$16.32, and the fixers are about \$5.10. Hence, taking the peak power of 1.178 W achieved by this passive fuel cell stack into consideration, the cost normalized by power output of this passive fuel cell stack is about \$60.08 W^{-1}. Comparing to the cost of an active DMFC stack, which is \$43.19 W^{-1} [48], the cost of this passive fuel cell stack is higher, which is attributed to the high cathode catalyst loading. All the results show that the passive stack is a promising candidate to be further studied for future application.

4.2. Effect of the ethylene glycol concentration

The effect of the EG concentration on the passive stack performance was studied as shown in Figs. 4 (a) and (b). In addition to the variations EG concentrations from 1.0 M to 7.0 M, the concentrations of KOH, H_2O_2, and H_2SO_4 were fixed at 9.0 M, 4.0 M and 1.0 M, respectively. Meanwhile, the operating temperature was room temperature, and a pretreated Nafion 211 membrane was used as the cation exchange membrane. Fig. 4 (a) presents the polarization curves of the stack with different concentrations of EG. The peak power increased at first and then decreased with the increasing concentrations of EG from 1.0 M to 7.0 M, and the maximum value of the peak power reached 1178 mW with 5.0 M EG. At the same time, the values of the maximum current showed a large variation. The maximum current was 480 mA with 1.0 M EG. Then, it increased to around 860 mA when the concentration of EG was increased to 3.0 M and 5.0 M. However, with EG concentration further increasing to 7.0 M, the maximum current decreased to 590 mA. Moreover, as presented in Fig. 4 (b), the OCV increased from 2.89 V to 3.00 V with concentration of EG increasing from 1.0 M to 5.0 M. However, the OCV was reduced to 2.85 V at a EG concentration of 7.0 M. These observations of stack performance with different concentrations of EG can be explained by these reasons.

When the EG concentration varies from 1.0 M to 5.0 M, the diffusion of EG is promoted due to the increasing concentration gradient of EG, which results in an elevation of EG concentration on the anode CL from the starvation state to the sufficient state. Therefore, the OCV is elevated with the increasing EG concentration from 1.0 M to 5.0 M This explanation is also validated by the sharp decrease of voltage and power at the high current region of 480 mA with 1.0 M EG, which is caused by the severe concentration loss due to the fuel shortage. However, when the EG concentration was increased to 3.0 M and 5.0 M, the concentration losses at high current region became less severer. When the concentration of EG was further increased to 7.0 M, the stack performance experienced a significant degradation ascribed to three possible reasons. Firstly, competitive adsorption between EG and OH^- on the active sites occurs with a high EG concentration. When the concentration of EG is 7.0 M, the active sites on the anode CL are taken up by the EG, which hinders the adsorption of OH^- and results in a lower kinetics of EGOR. The sharp decrease of cell voltage with 7.0 M EG at a high current region of 590 mA is caused by the severe concentration loss due to the OH^- shortage, which validates the above explanation. Secondly, the crossover of EG becomes severer with a higher EG concentration. Although the EG permeated to the cathode cannot produce the mixed potential due the fact that Au is not sensitive to EG, a portion of active sites on the cathode CL is occupied by the EG. The reaction kinetics of HPRR is negatively affected, which is reflected by the decreased OCV of the cell stack with EG concentration increasing from 5.0 M to 7.0 M as shown in Fig. 4 (b). Lastly, the viscosity of anolyte increases as EG concentration increases. The transportation of the reactants and charges is hindered, which results in a larger internal resistance and an elevated ohmic loss as shown in Fig. 4 (b). In summary, the passive stack outputs the maximum OCV, current, and power of 3.0 V, 860 mA, and 1178 mW, respectively, at an EG concentration of 5.0 M when other operating conditions are constant.

4.3. Effect of the hydroxide−ion concentration

Fig. 5 (a) shows the effect of the KOH concentration on the stack performance with EG, H_2O_2, and H_2SO_4 concentrations fixed at 5.0, 4.0, and 1.0 M accordingly. It can be observed that the OCV increased from 2.68V to 3.06V with OH^- concentration increasing from 5.0 M to 11.0 M. In terms of a specific catalyst, the kinetics of EGOR is dominated by the local concentrations of species in the anode CL. At an EG concentration of 5.0 M, a higher OH^- feeding concentration will result in enhanced OH^- transportation from the anode reservoir to the anode CL where a starvation state of OH^- is transferred to a sufficient state. Therefore, the EGOR kinetics is enhanced through this process, which leads to a gradually increasing OCV as presented in Fig. 5 (b). However, the gradient of the OCV curve in Fig. 5 (b) was smaller, indicating that further increasing the OH^- concentration had little contribution to the enhancement of OCV. This can be explained that the adsorption of OH^- has almost been saturated at the concentration of 9.0 M, thus limited OH^- is able to be adsorbed on the active sites. It can be obtained that the peak power of 1178 mW was reached at 9.0 M as presented in Fig. 5 (a), while the performance would degrade with either higher or lower OH^- concentration. Generally, the electrochemical kinetics and the species transport in the anode largely depend on the alkalinity of the anode. It can be observed from Fig. 5 (b) that the internal resistance enlarged from 285 mOhm to 316 mOhm when OH^- concentration increased from 5.0 M to 9.0 M. The performance is still improved because the compensation of positive effect of facilitated EGOR kinetics on stack performance for the increased ohmic loss is adequate. When further increasing the OH^- concentration, the internal resistance increasing to 331 mOhm led to a larger ohmic loss. In addition, the active sites will be fully occupied by OH^-, hence the EGOR kinetics is reduced and the concentration loss is promoted. In conclusion, the performance of the passive stack improves with OH^- concentration increasing from 5.0 M to 9.0 M, then declines with OH^- concentration increasing from 9.0 M to 11.0 M.

4.4. Effect of the hydrogen peroxide concentration

The H_2O_2 used in the cathode acts as the oxidant for the passive stack, and its concentration plays a crucial role on the stack performance. As shown in Figs. 6 (a) and (b), the effect of H_2O_2 concentration on stack performance was investigated with a constant H_2SO_4 concentration at 1.0 M. In Fig. 6 (a), it could be seen from the polarization curves with different H_2O_2 concentrations that the stack performance was improved as the H_2O_2 concentration was first elevated from 2.0 M to 4.0 M, then degraded with H_2O_2 concentration further increasing to 6.0 M. The stack voltage in the whole current region increased first and then decreased with the increasing concentration of H_2O_2 and the maximum current also conformed to the same trend. The best performance was obtained when the concentration of H_2O_2 was 4.0 M with a highest power of 1178 mW and a maximum current of 860 mA. Fig. 6 (b) shows that the OCV of the stack experienced an increase from 2.92 V to 3.00 V with H_2O_2 concentration increasing from 2.0 M to 4.0 M, and then decreasing to 2.79 V as H_2O_2 concentration further reached 4.0 M. Meanwhile, the internal resistance of the stack enlarged from 331 mOhm to 368 mOhm with the increased concentration of H_2O_2. The above observations can be explained as follows. As shown in Fig. 6 (a), the significant concentration loss at high current range with the H_2O_2 concentration of 2.0 M reveals the fact that the local concentration of H_2O_2 on cathode CL is in a deficient state. As the concentration of H_2O_2 increases from 2.0 M to 4.0 M, the diffusion of H_2O_2 to the CL is promoted and the concentration of H_2O_2 on the CL is transferred from a deficient state to a sufficient state. Meanwhile, the kinetics of HPRR is much improved. Thus, the OCV of the stack increases in this process as presented in Fig. 6 (b), and the stack performance is improved. However, with the H_2O_2 concentration further increasing to 6.0 M, the OCV decreases and the stack performance degrades as well. This phenomenon can be attributed to three aspects. Firstly, the excessively high concentration of H_2O_2 leads to the competitive adsorption between H_2O_2 and H^+ on the active sites of cathode CL. The adsorption of H^+ becomes insufficient and the kinetics of HPRR becomes lower, which is also reflected

by the sharp decrease of the stack voltage in high current region. Secondly, with a higher H_2O_2 concentration, the self-decomposition of H_2O_2 becomes severer, which produces a larger number of gaseous products in the cathode. The gas bubbles presented in the electrolyte reservoir may impede the transport of H_2O_2 and H_2SO_4 to the cathode CL and leads to an increasing internal resistance of the stack as presented in Fig. 6 (b). Last but not least, the crossover of H_2O_2 from the cathode to anode is severer with a higher concentration. At the same time, the transport of EG and KOH in the anode may also be influenced by the gaseous products produced by the self-decomposition of the H_2O_2 in the anode, which produces negative impact on the stack performance as well.

4.5. Effect of the sulfuric acid concentration

Fig. 7 (a) presents the effect of the H_2SO_4 concentration on the passive stack performance with EG, H_2O_2, and KOH concentrations fixed at 5.0, 4.0, and 9.0 M, respectively. It can be observed that the OCV increased from 2.85 V to 3.01 V with H_2SO_4 concentration increasing from 0.5 M to 1.0 M and decreased from 3.01 V to 2.86 V with H_2SO_4 concentration further increasing from 1.0 M to 2.0 M. This phenomenon can be accounted as follows. With H_2SO_4 concentration increasing from 0.5 M to 1.0 M, the increasing voltage is resulted from the enhanced transportation of H^+ which weakens the concentration loss of H^+ [49]. However, further increasing H_2SO_4 concentration to 2.0 M did not lead to a better performance. One reason is that the redundant H_2SO_4 have taken up numerous active sites, which results in shortage of H_2O_2 in the CL. Then a higher H_2O_2 concentration loss is caused and the voltage degrades. Another reason is that the viscosity of catholyte is enlarged due to the increasing H_2SO_4 concentration. Meanwhile, the internal resistance rises when H_2SO_4 concentration increases as shown in Fig. 7 (b), which then causes severer ohmic loss. Therefore, the passive stack has the best performance with H_2SO_4 concentration at 1.0 M.

In summary, the reasons why the fuel cell performance will drop at higher feeding-concentrations of reactants can be concluded as follows: (1) the competitive adsorption between the reactants on active sites results in the lowered reaction kinetics and the increased concentration loss; (2) the viscosity of electrolyte becomes larger, impeding the transportation of reactants and charges; and (3) the hindered delivery of reactants leads to a larger internal resistance and an increased ohmic loss.

4.6. Demonstration of the passive stack to power an underwater fan

As mentioned, one advantage of the passive stack using hydrogen oxide is the feasibility to be a power source for underwater and outer space applications where the air is insufficient. Therefore, this superiority is emphasized by comparing the capacity of the passive stack powering an electric fan with different oxidants, i.e., hydrogen peroxide and air, under different working circumstances, i.e., normal environment and mimetic underwater environment. The fuel cell stack is operated with 5.0 M EG and 9.0 M KOH as anolyte and 4.0 M H_2O_2 and 1.0 M H_2SO_4 as catholyte at room temperature. The capacity is verified by the running time of the fan, whose power rating and revolutions per minute are 1.8 W and 20000 rpm, respectively. Under the normal environment, after the connection of the anode and cathode of the stack and the fan by wires, the fan could not run when the passive stack used the ambient air as oxidant. This is because that the Au based cathode is not able to catalyze the ORR effectively, thus the power output is unable to drive the fan. On the contrary, when the hydrogen peroxide was used, the fan rotated at a high speed. To present the continuous output ability of the passive stack, a stopwatch was used to measure how long the fan would run until the fan gradually slowed down and completely stopped. It can be observed from Fig. 8 (a) that the whole running time was 2 hours and 52 minutes, indicating that the passive stack possesses the potential for practical applications. As shown in Fig. 8 (b), to further imitate the underwater environment without air supply, an airtight condition was created by a sealed box within the stack and fan,

which was placed in a larger box full of water. It is found that the whole running time of the fan was 2 hours and 36 minutes underwater, which was similar to the result in the natural circumstance. The satisfactory performance under the underwater condition demonstrates that the passive stack is an applicable power source and has the potential for future application in relevant fields.

5. Concluding remarks

In this study, a passive direct ethylene glycol fuel cell stack is proposed, fabricated, and tested. This passive design reduces the volume and weight of the stack comparing to the active fuel cell stack, thus both specific energy density and volumetric energy density are improved. The effect of feeding species concentrations on the stack performance is studied. The results indicate that the peak power of this passive stack is 1178 mW at room temperature with the optimal reactant-feeding concentrations of 5.0 M EG and 9.0 M KOH as anolyte and 4.0 M H_2O_2 and 1.0 M H_2SO_4 as catholyte. The achieved peak power density is twice as high as that of a passive cell using ethylene glycol as fuel and air as oxidant. The impressive improvement results from the faster hydrogen peroxide reduction reaction due to its two-electron-transfer process rather than the four-electron-transfer process. In addition, the individual cell in the passive stack exhibits a good consistency over the whole current region, indicating a high degree of reproducibility achieved by the appropriate electrode manufacturing process. Moreover, to demonstrate the passive stack to be a promising power source under special situations, such as underwater and outer space, the passive stack is applied to power an electric fan under the mimetic underwater environment. It is demonstrated that the whole running time of the electric fan is 2 hours and 36 minutes with hydrogen peroxide as oxidant, while the air is used as oxidant, the electric fan is unable to run, suggesting that this passive stack can be applied in situations where air is insufficient.

Acknowledgement:

This work was fully supported by a grant from the Research Grants Council of the Hong Kong Special Administrative Region, China (Project No. 25211817).

References

[1] Z.F. Pan, L. An, T.S. Zhao, Z.K. Tang, Advances and challenges in alkaline anion exchange membrane fuel cells, Progress in Energy and Combustion Science 66 (2018) 141-175.

[2] Q.X. Wu, Z.F. Pan, L. An, Recent advances in alkali-doped polybenzimidazole membranes for fuel cell applications, Renewable and Sustainable Energy Reviews 89 (2018) 168-183.

[3] Z.F. Pan, L. An, C.Y. Wen, Recent advances in fuel cells based propulsion systems for unmanned aerial vehicles, Applied Energy 240 (2019) 473-485.

[4] Y. Li, Y. Feng, X. Sun, Y. He, A Sodium-Ion-Conducting Direct Formate Fuel Cell: Generating Electricity and Producing Base, Angewandte Chemie International Edition 56 (2017) 5734-5737.

[5] B. Huang, Z. Pan, X. Su, L. An, Tin-based materials as versatile anodes for alkali (earth)-ion batteries, Journal of Power Sources 395 (2018) 41-59.

[6] S. Rousseau, C. Coutanceau, C. Lamy, J.M. Léger, Direct ethanol fuel cell (DEFC): Electrical performances and reaction products distribution under operating conditions with different platinum-based anodes, Journal of Power Sources 158 (2006) 18-24.

[7] Y. Li, X. Sun, Y. Feng, Hydroxide Self-Feeding High-Temperature Alkaline Direct Formate Fuel Cells, ChemSusChem 10 (2017) 2135-2139.

[8] T.S. Zhao, C. Xu, R. Chen, W.W. Yang, Mass transport phenomena in direct methanol fuel cells, Progress in Energy and Combustion Science 35 (2009) 275-292.

[9] L. An, T.S. Zhao, Transport phenomena in alkaline direct ethanol fuel cells for sustainable energy production, Journal of Power Sources 341 (2017) 199-211.

[10] Y. Li, Y. Feng, X. Sun, Insight into Interface Behaviors to Build Phase-Boundary-Matched Na-Ion Direct Liquid Fuel Cells, ACS Sustainable Chemistry & Engineering 6 (2018) 12827-12834.

[11] V. Livshits, M. Philosoph, E. Peled, Direct ethylene glycol fuel-cell stack—study of oxidation intermediate products, Journal of Power Sources 178 (2008) 687-691.

[12] L. An, R. Chen, Recent progress in alkaline direct ethylene glycol fuel cells for sustainable energy production, Journal of Power Sources 329 (2016) 484-501.

[13] A. Serov, C. Kwak, Recent achievements in direct ethylene glycol fuel cells (DEGFC), Applied Catalysis B: Environmental 97 (2010) 1-12.

[14] H. Yue, Y. Zhao, X. Ma, J. Gong, Ethylene glycol: properties, synthesis, and applications, Chemical Society Reviews 41 (2012) 4218-4244.

[15] J. Qi, N. Benipal, C. Liang, W. Li, PdAg/CNT catalyzed alcohol oxidation reaction for high-performance anion exchange membrane direct alcohol fuel cell (alcohol=methanol, ethanol, ethylene glycol and glycerol), Applied Catalysis B: Environmental 199 (2016) 494-503.

[16] R. Kannan, A.R. Kim, J.S. Kim, D.J. Yoo, 3D graphene-mixed metal oxide-supported carbonpalladium quantum dot nanoarchitectures – A facile bifunctional electrocatalyst for direct ethylene glycol fuel cells and oxygen evolution reactions, International Journal of Hydrogen Energy 41 (2016) 18033-18043.

[17] O.O. Fashedemi, H.A. Miller, A. Marchionni, F. Vizza, K.I. Ozoemena, Electro-oxidation of ethylene glycol and glycerol at palladium-decorated FeCo@Fe core–shell nanocatalysts for alkaline direct alcohol fuel cells: functionalized MWCNT supports and impact on product selectivity, Journal of Materials Chemistry A 3 (2015) 7145-7156.

[18] Z.F. Pan, R. Chen, L. An, Y.S. Li, Alkaline anion exchange membrane fuel cells for cogeneration of electricity and valuable chemicals, Journal of Power Sources 365 (2017) 430-445.

[19] T. Luo, S. Abdu, M. Wessling, Selectivity of ion exchange membranes: A review, Journal of membrane science 555 (2018) 429-454.

[20] L. An, T. Zhao, Q. Wu, L. Zeng, Comparison of different types of membrane in alkaline direct ethanol fuel cells, International Journal of Hydrogen Energy 37 (2012) 14536-14542.

[21] L. An, T.S. Zhao, S.Y. Shen, Q.X. Wu, R. Chen, Performance of a direct ethylene glycol fuel cell with an anion-exchange membrane, International Journal of Hydrogen Energy 35 (2010) 4329-4335.

[22] L. An, L. Zeng, T.S. Zhao, An alkaline direct ethylene glycol fuel cell with an alkali-doped polybenzimidazole membrane, International Journal of Hydrogen Energy 38 (2013) 10602-10606.

[23] Y. Feng, L. Bu, S. Guo, J. Guo, X. Huang, 3D Platinum–Lead Nanowire Networks as Highly Efficient Ethylene Glycol Oxidation Electrocatalysts, Small 12 (2016) 4464-4470.

[24] Z. Pan, Y. Bi, L. An, Mathematical modeling of direct ethylene glycol fuel cells incorporating the effect of the competitive adsorption, Applied Thermal Engineering 147 (2019) 1115-1124.

[25] E. Peled, V. Livshits, T. Duvdevani, High-power direct ethylene glycol fuel cell (DEGFC) based on nanoporous proton-conducting membrane (NP-PCM), Journal of Power Sources 106 (2002) 245-248.

[26] Y.-C. Shi, J.-J. Feng, X.-X. Lin, L. Zhang, J. Yuan, Q.-L. Zhang, A.-J. Wang, One-step hydrothermal synthesis of three-dimensional nitrogen-doped reduced graphene oxide hydrogels anchored PtPd alloyed nanoparticles for ethylene glycol oxidation and hydrogen evolution reactions, Electrochimica Acta 293 (2019) 504-513.

[27] Z.-N. Yu, Z. Zhang, Z.-S. Lv, M.-T. Liu, L. Zhang, A.-J. Wang, L.-Y. Jiang, J.-J. Feng, Platinum69-cobalt31 alloyed nanosheet nanoassemblies as advanced bifunctional electrocatalysts for boosting ethylene glycol oxidation and oxygen reduction, Journal of Colloid and Interface Science 525 (2018) 216-224.

[28] X.-Y. Huang, A.-J. Wang, X.-F. Zhang, L. Zhang, J.-J. Feng, One-step synthesis of PtCu alloyed nanocages with highly open structures as bifunctional electrocatalysts for oxygen reduction and polyhydric alcohol oxidation, ACS Applied Energy Materials 1 (2018) 5779-5786.

[29] Z. Pan, B. Huang, L. An, Performance of a hybrid direct ethylene glycol fuel cell, International Journal of Energy Research 43 (2019) 2583-2591.

[30] Y. Li, A liquid-electrolyte-free anion-exchange membrane direct formate-peroxide fuel cell, International Journal of Hydrogen Energy 41 (2016) 3600-3604.

[31] I. Chino, K. Hendrix, A. Keramati, O. Muneeb, J.L. Haan, A split pH direct liquid fuel cell powered by propanol or glycerol, Applied Energy 251 (2019) 113323.

[32] T. Zhao, C. Xu, R. Chen, W. Yang, Mass transport phenomena in direct methanol fuel cells, Progress in Energy and Combustion Science 35 (2009) 275-292.

[33] C. Cremers, A. Niedergesäß, F. Jung, D. Müller, J. Tübke, Development of an Alkaline Anion Exchange Membrane Direct Ethylene Glycol Fuel Cell Stack, ECS Transactions 41 (2011) 1987-1996.

[34] J.P. Pereira, D.S. Falcão, V.B. Oliveira, A.M.F.R. Pinto, Performance of a passive direct ethanol fuel cell, Journal of Power Sources 256 (2014) 14-19.

[35] Y.S. Li, T.S. Zhao, A passive anion-exchange membrane direct ethanol fuel cell stack and its applications, International Journal of Hydrogen Energy 41 (2016) 20336-20342.

[36] S.S. Munjewar, S.B. Thombre, R.K. Mallick, Approaches to overcome the barrier issues of passive direct methanol fuel cell – Review, Renewable and Sustainable Energy Reviews 67 (2017) 1087-1104.

[37] Z. Pan, Y. Bi, L. An, Performance characteristics of a passive direct ethylene glycol fuel cell with hydrogen peroxide as oxidant, Applied Energy 250 (2019) 846-854.

[38] A. Marchionni, M. Bevilacqua, C. Bianchini, Y.X. Chen, J. Filippi, P. Fornasiero, A. Lavacchi, H. Miller, L. Wang, F. Vizza, Electrooxidation of Ethylene Glycol and Glycerol on Pd-(Ni-Zn)/C Anodes in Direct Alcohol Fuel Cells, ChemSusChem 6 (2013) 518-528.

[39] O.O. Fashedemi, H.A. Miller, A. Marchionni, F. Vizza, K.I. Ozoemena, Electro-oxidation of ethylene glycol and glycerol at palladium-decorated FeCo@ Fe core–shell nanocatalysts for alkaline direct alcohol fuel cells: functionalized MWCNT supports and impact on product selectivity, Journal of Materials Chemistry A 3 (2015) 7145-7156.

[40] L. An, T. Zhao, R. Chen, Q. Wu, A novel direct ethanol fuel cell with high power density, Journal of Power Sources 196 (2011) 6219-6222.

[41] L. An, T.S. Zhao, Performance of an alkaline-acid direct ethanol fuel cell, International Journal of Hydrogen Energy 36 (2011) 9994-9999.

[42] A. Marchionni, M. Bevilacqua, C. Bianchini, Y.-X. Chen, J. Filippi, P. Fornasiero, A. Lavacchi, H. Miller, L. Wang, F. Vizza, Electrooxidation of Ethylene Glycol and Glycerol on Pd-(Ni-Zn)/C Anodes in Direct Alcohol Fuel Cells, ChemSusChem 6 (2013) 518-528.

[43] G.H. Miley, N. Luo, J. Mather, R. Burton, G. Hawkins, L. Gu, E. Byrd, R. Gimlin, P.J. Shrestha, G. Benavides, J. Laystrom, D. Carroll, Direct NaBH4/H2O2 fuel cells, Journal of Power Sources 165 (2007) 509-516.

[44] D. Noren, M. Hoffman, Clarifying the Butler–Volmer equation and related approximations for calculating activation losses in solid oxide fuel cell models, Journal of Power Sources 152 (2005) 175-181.

[45] J. Larminie, A. Dicks, M.S. McDonald, Fuel cell systems explained, J. Wiley Chichester, UK, 2003.

[46] T.R. Ralph, G.A. Hards, J.E. Keating, S.A. Campbell, D.P. Wilkinson, M. Davis, J. St-Pierre, M.C. Johnson, Low Cost Electrodes for Proton Exchange Membrane Fuel Cells: Performance in Single Cells and Ballard Stacks, Journal of The Electrochemical Society 144 (1997) 3845-3857.

[47] S.S. Pethaiah, J. Arunkumar, M. Ramos, A. Al-Jumaily, N. Manivannan, The impact of anode design on fuel crossover of direct ethanol fuel cell, Bulletin of Materials Science 39 (2016) 273-278.

[48] M. Sgroi, F. Zedde, O. Barbera, A. Stassi, D. Sebastián, F. Lufrano, V. Baglio, A. Aricò, J. Bonde, M. Schuster, Cost analysis of direct methanol fuel cell stacks for mass production, Energies 9 (2016) 1008.

[49] R.K. Raman, N.A. Choudhury, A.K. Shukla, A High Output Voltage Direct Borohydride Fuel Cell, Electrochemical and Solid-State Letters 7 (2004) A488-A491.

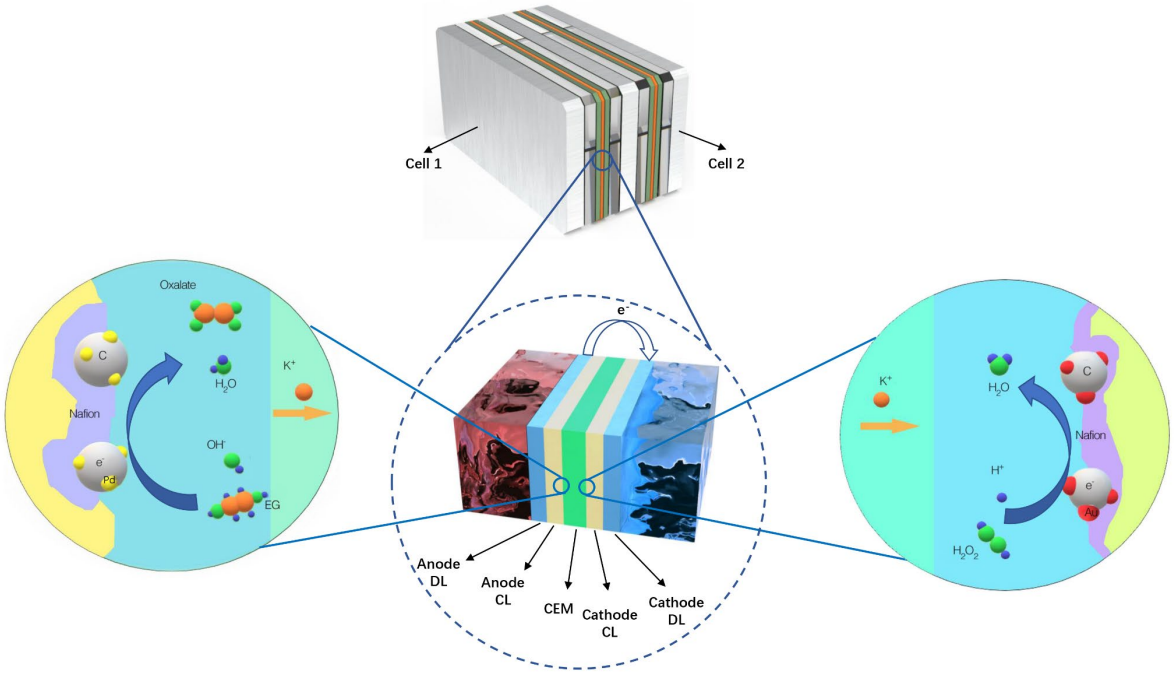

Fig. 1 (a) Working principle of a passive DEGFC stack

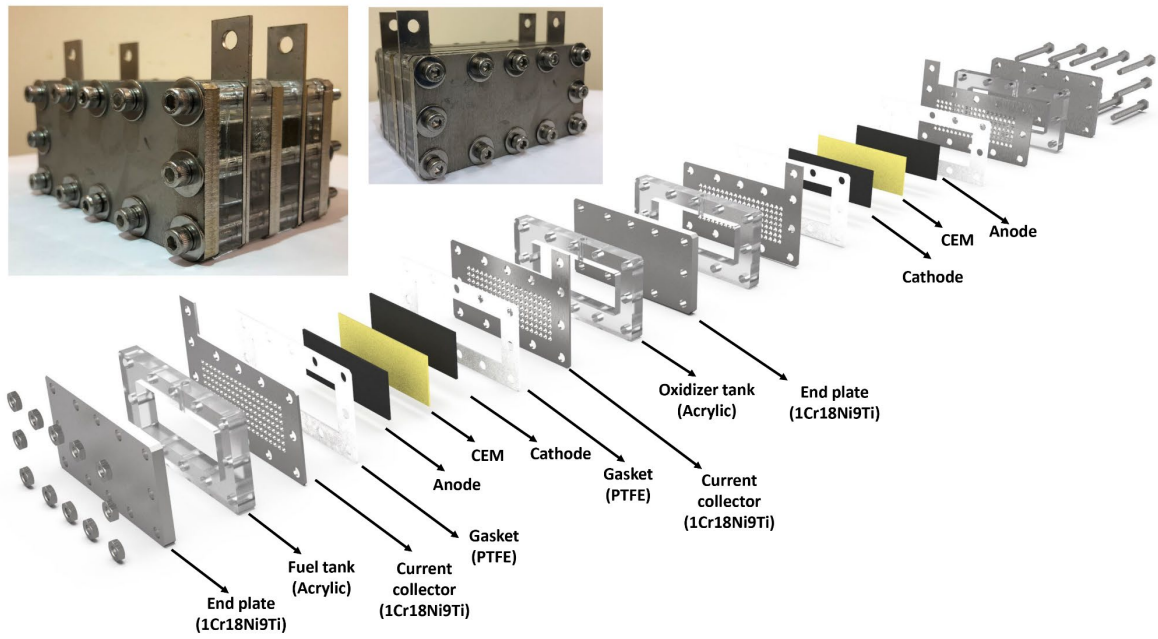

Fig. 1 (b) Schematic illustration of a passive DEGFC stack.

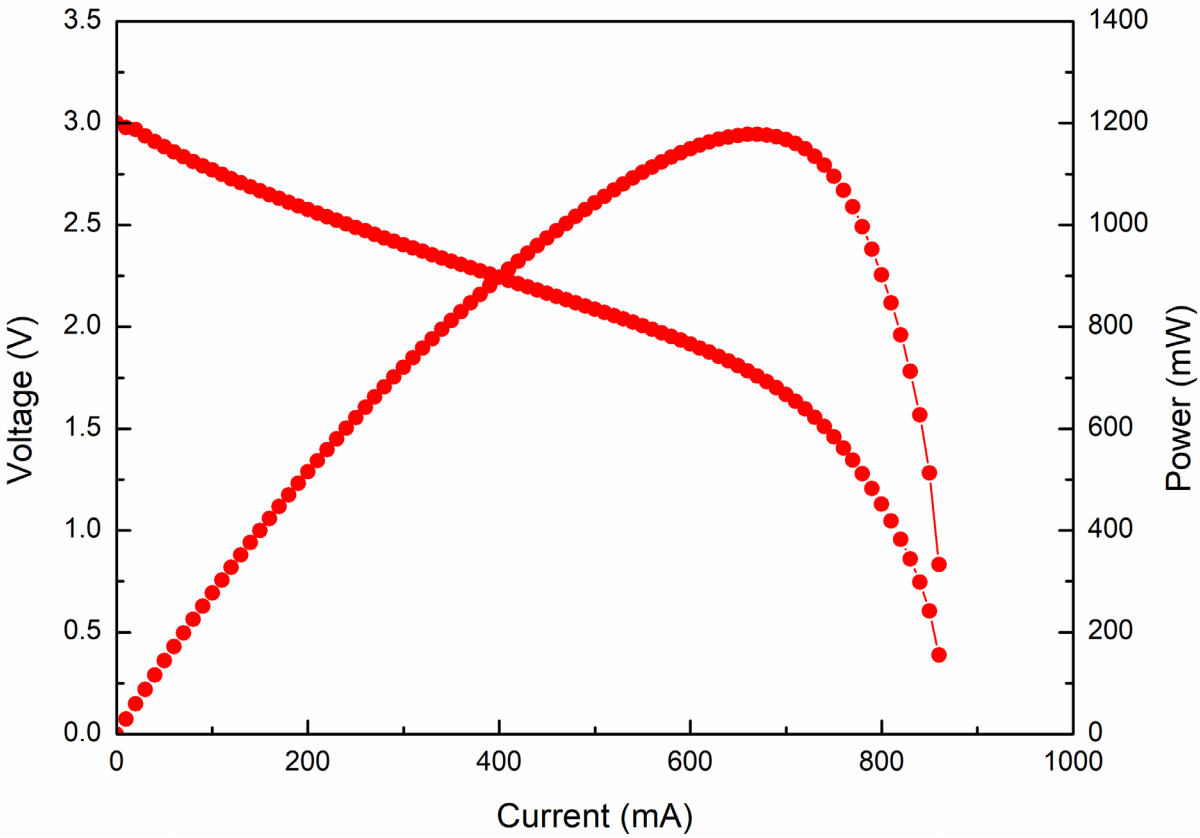

Fig. 2 (a) General Performance of the passive stack.

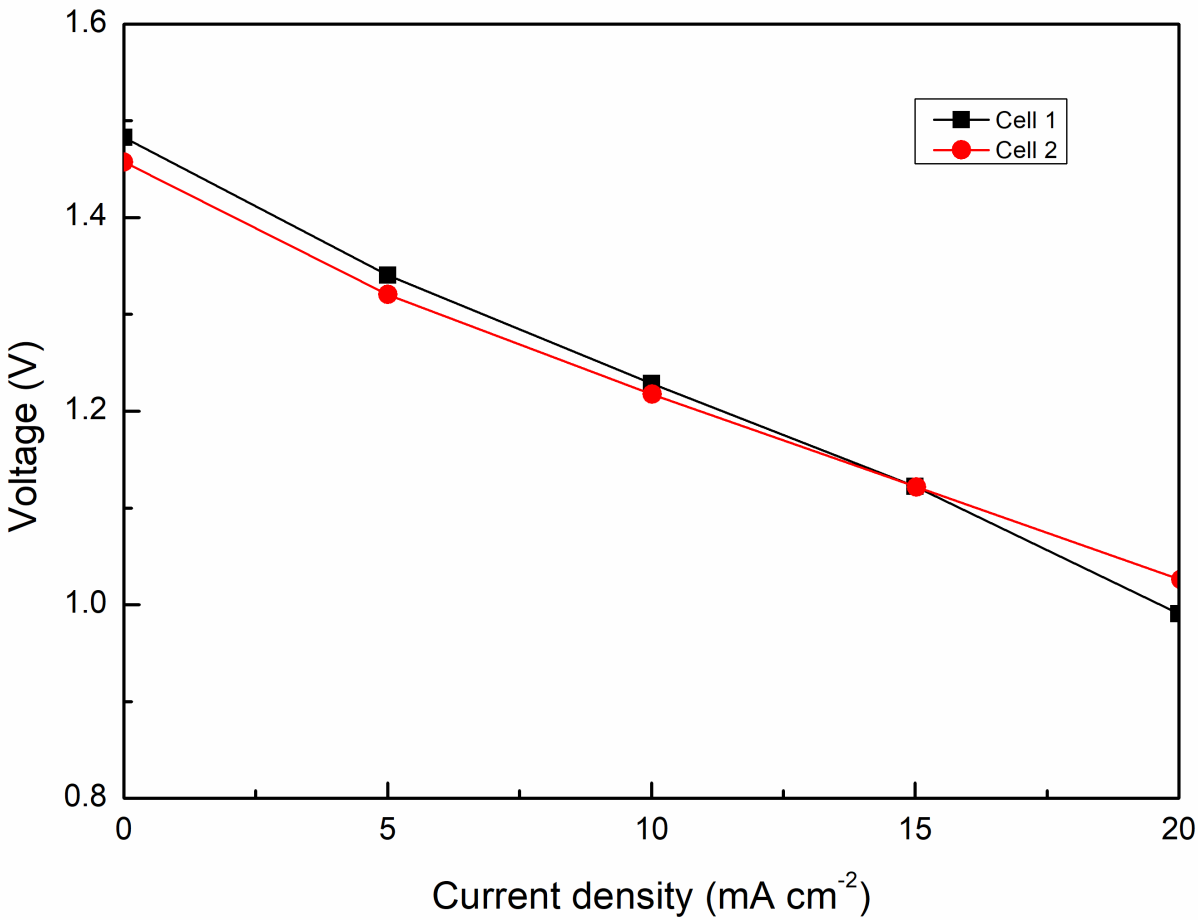

Fig. 2 (b) The consistency of the individual cell.

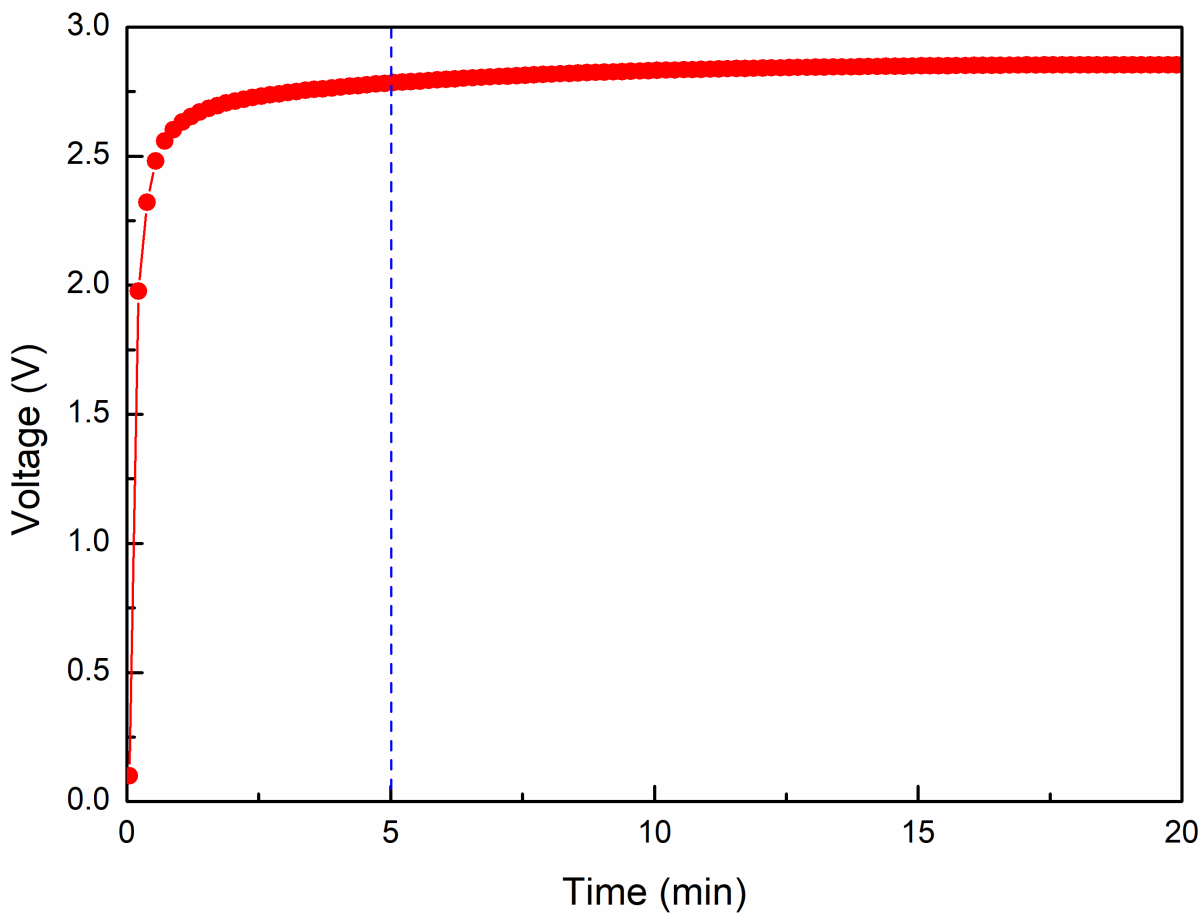

Fig. 3 (a) Transient OCV behavior of the passive stack.

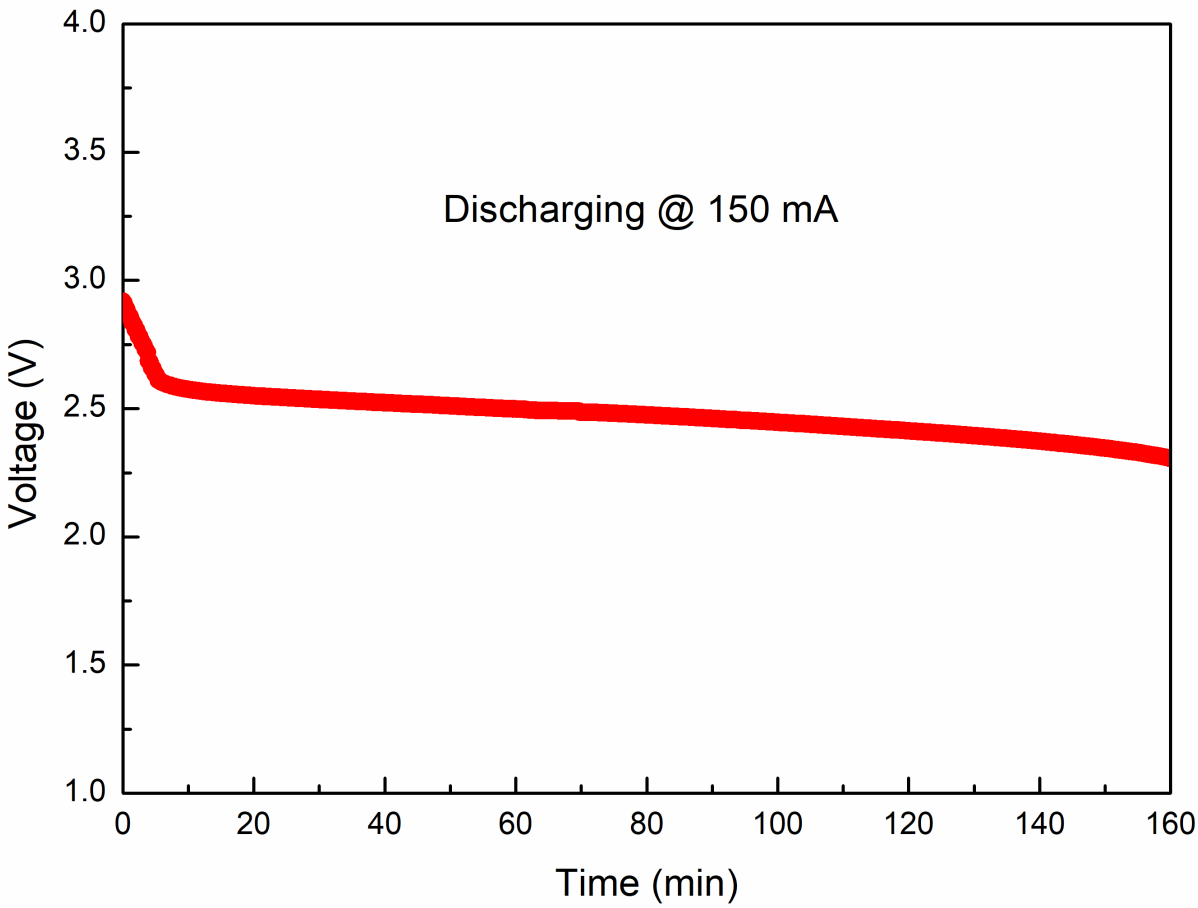

Fig. 3 (b) Transient discharging behavior of the passive stack.

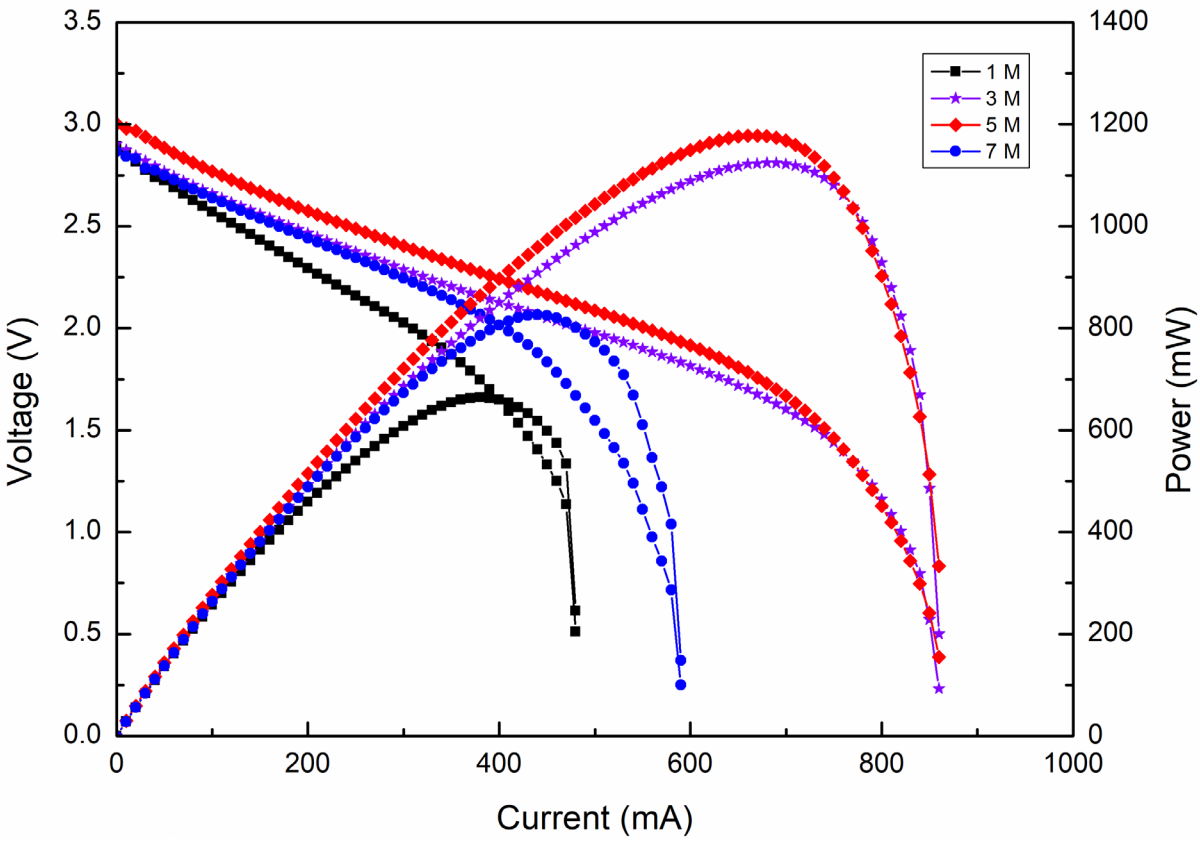

Fig. 4 (a) Effect of the EG concentration on the stack performance.

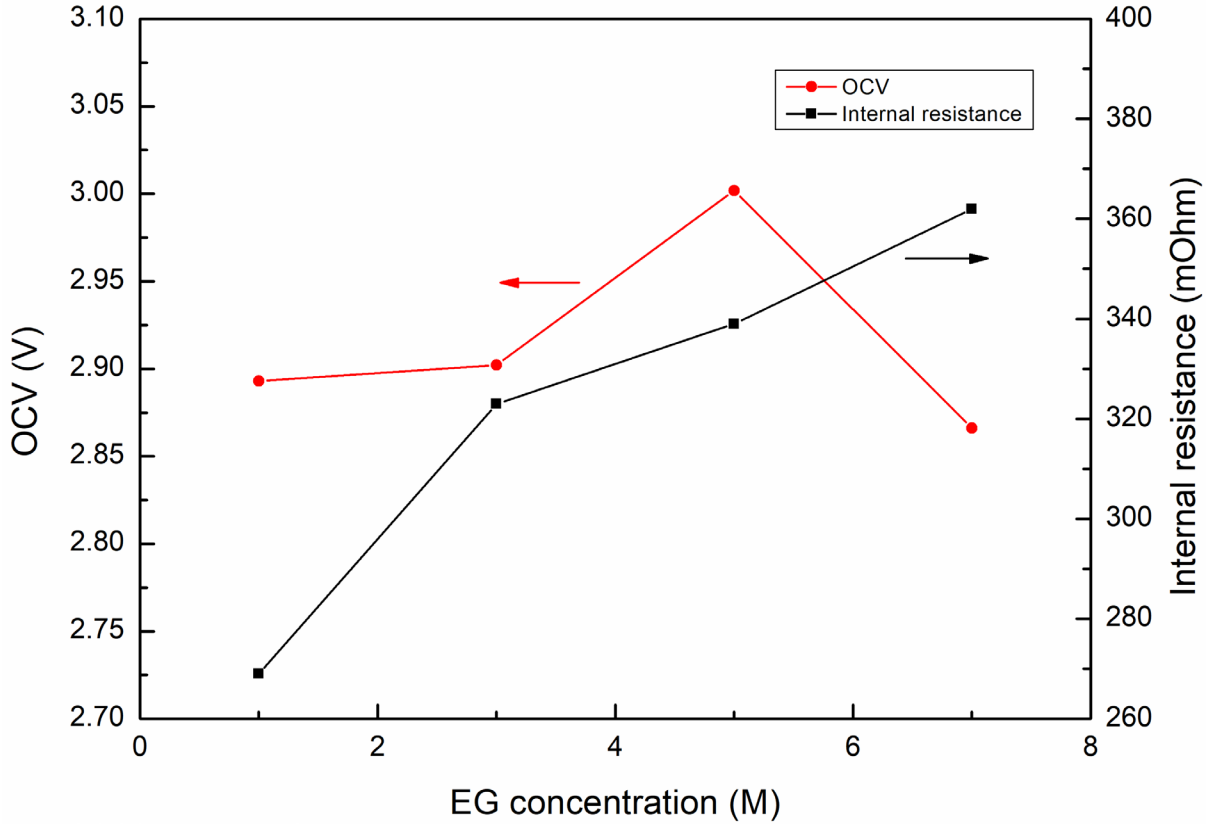

Fig. 4 (b) Effect of the EG concentration on the OCV and internal resistance.

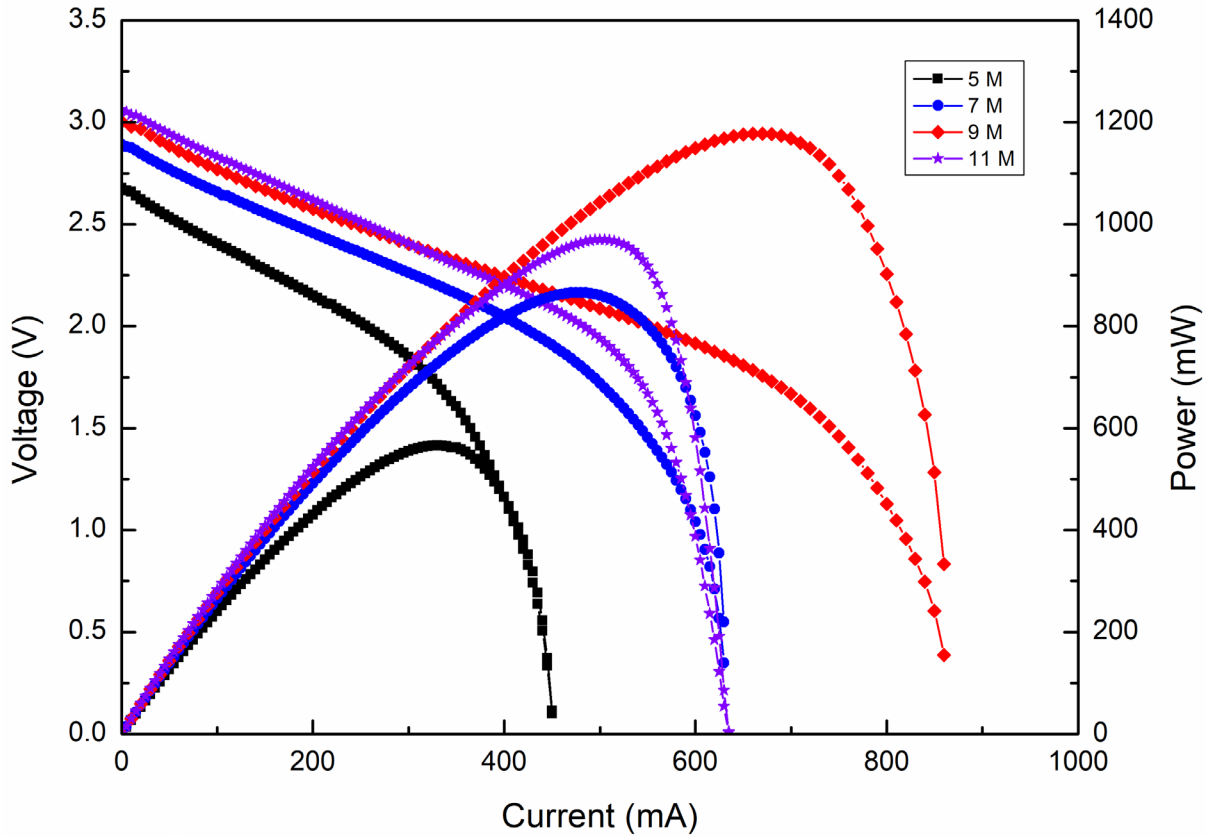

Fig. 5 (a) Effect of the KOH concentration on the stack performance.

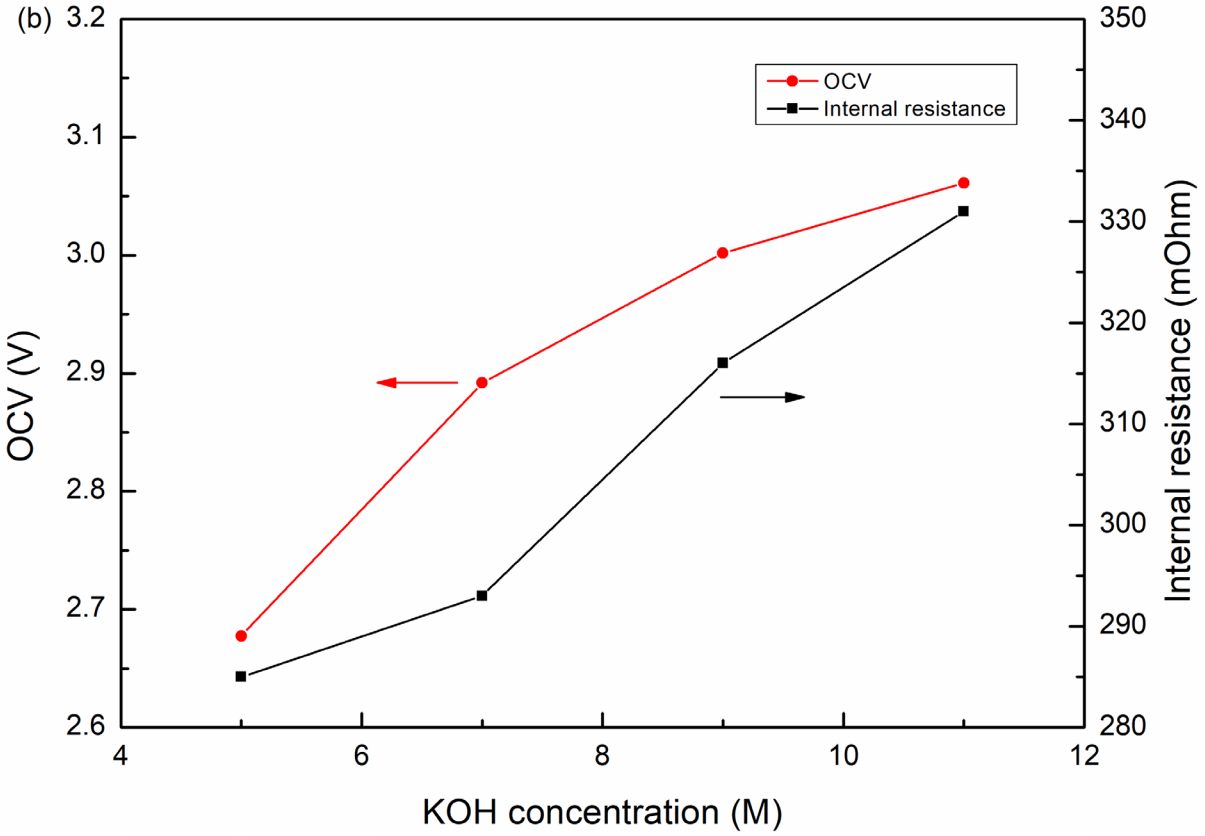

Fig. 5 (b) Effect of the KOH concentration on the OCV and internal resistance.

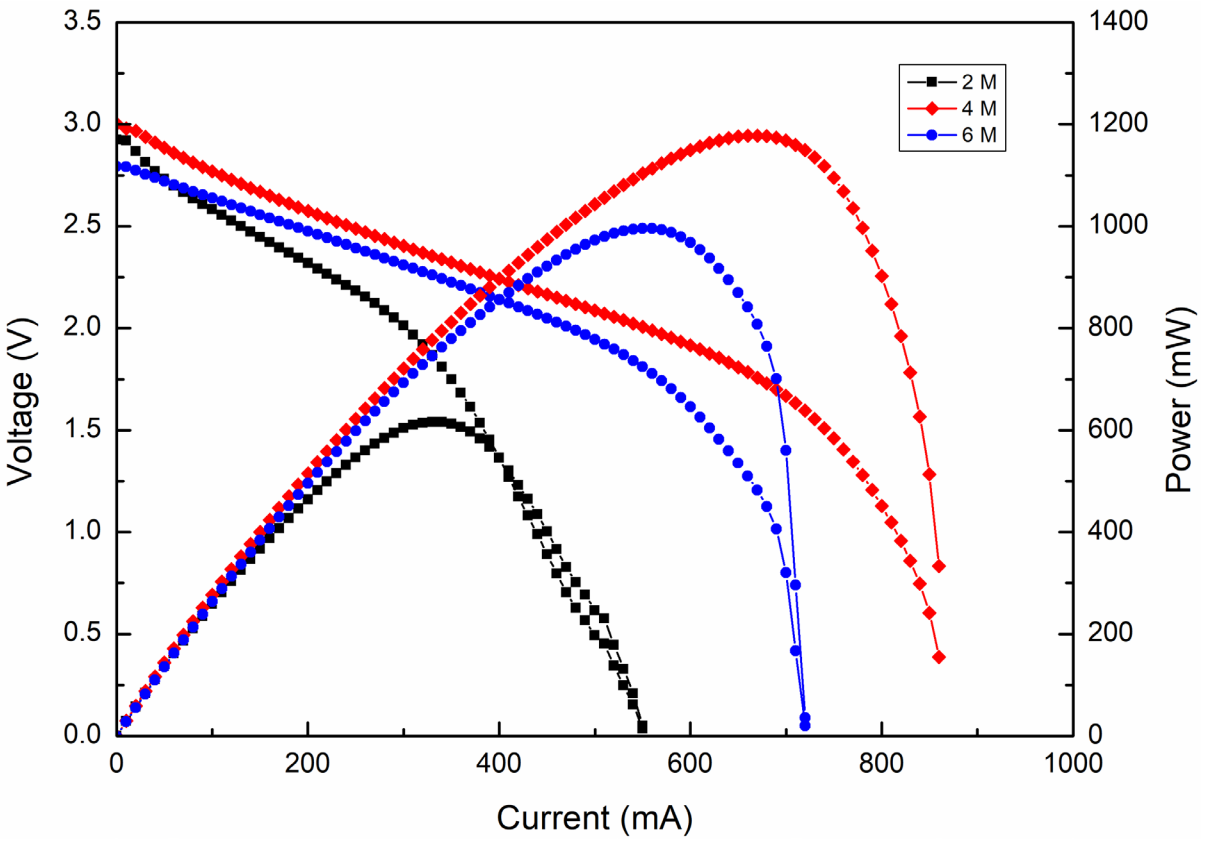

Fig. 6 (a) Effect of the H_2O_2 concentration on the stack performance.

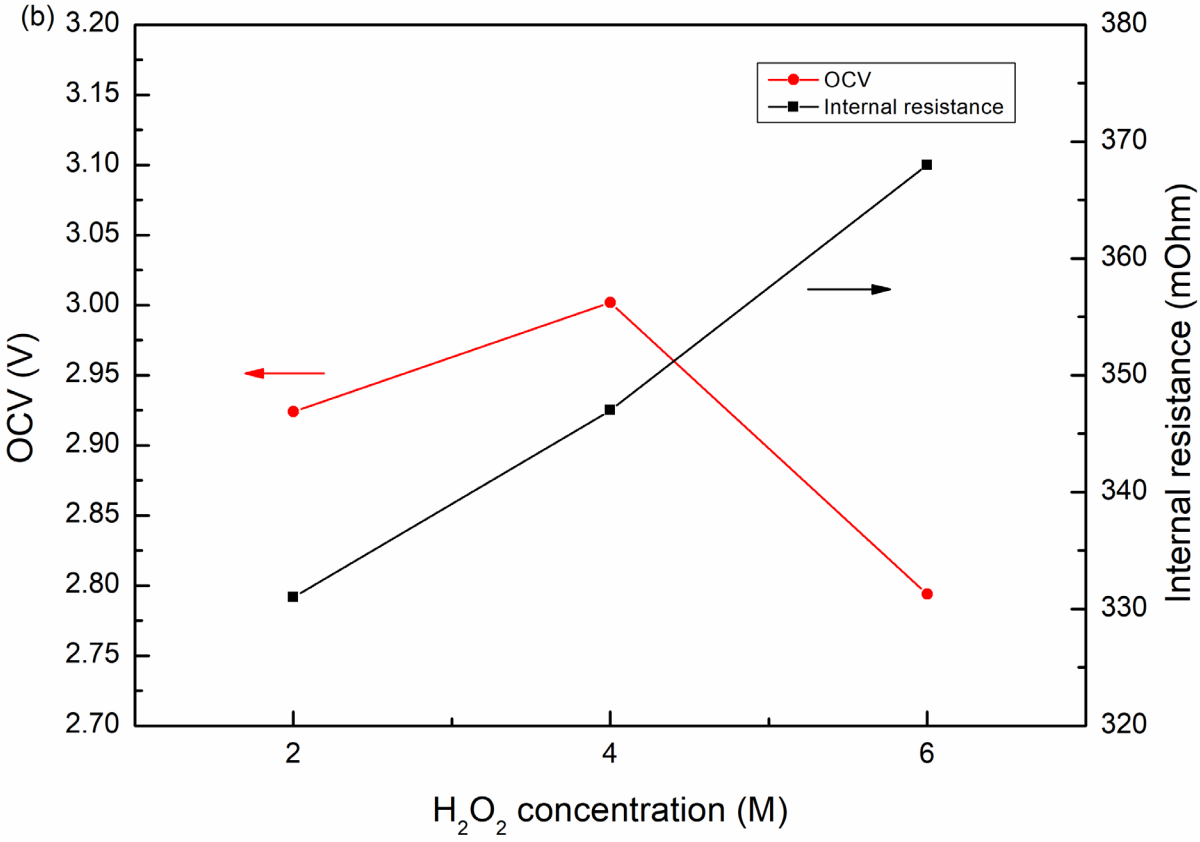

Fig. 6 (b) Effect of the H_2O_2 concentration on the OCV and internal resistance.

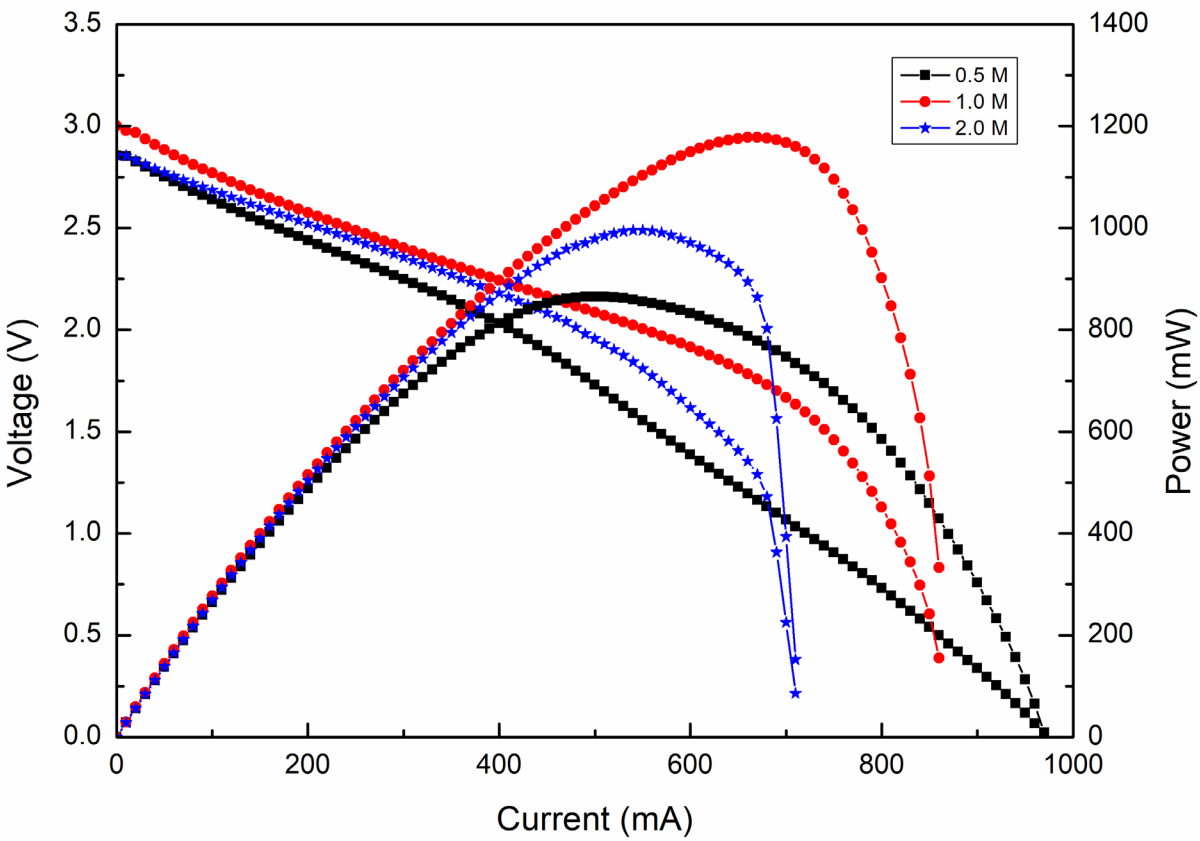

Fig. 7 (a) Effect of the H_2SO_4 concentration on the stack performance.

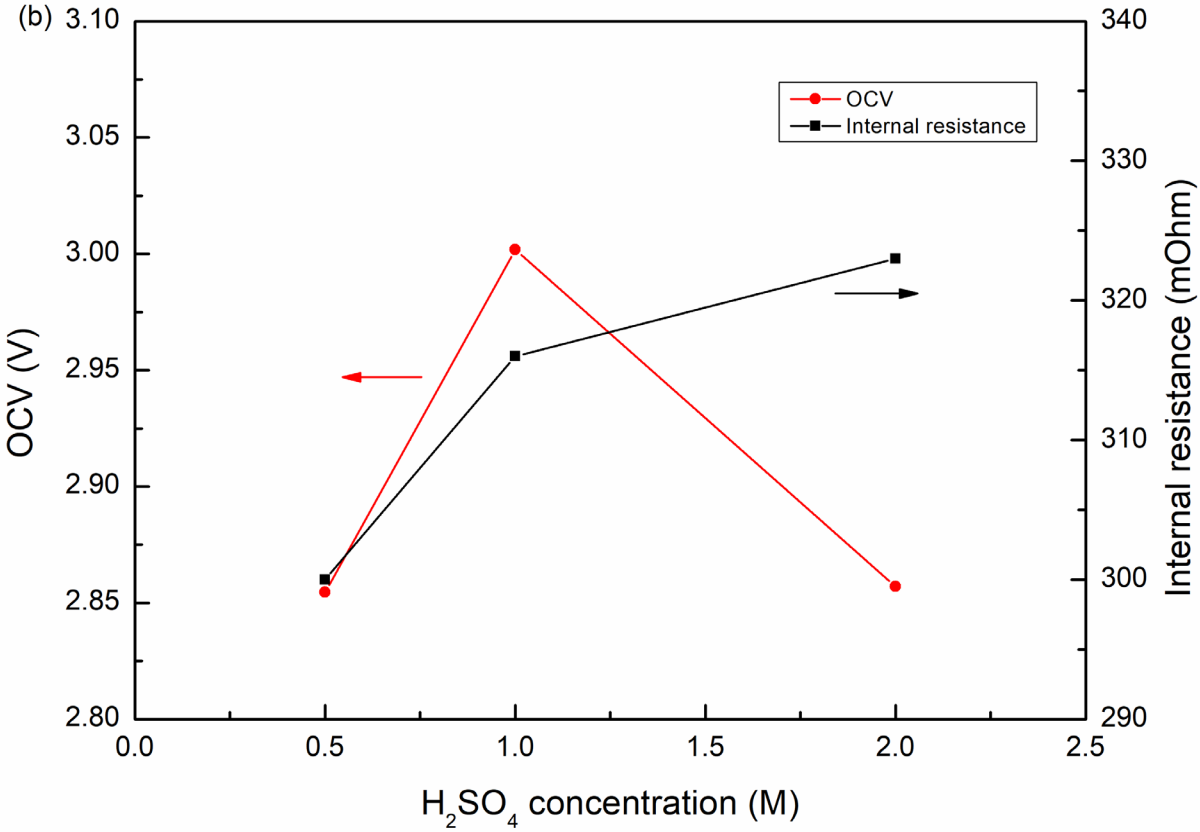

Fig. 7 (b) Effect of the H_2SO_4 concentration on the OCV and internal resistance.

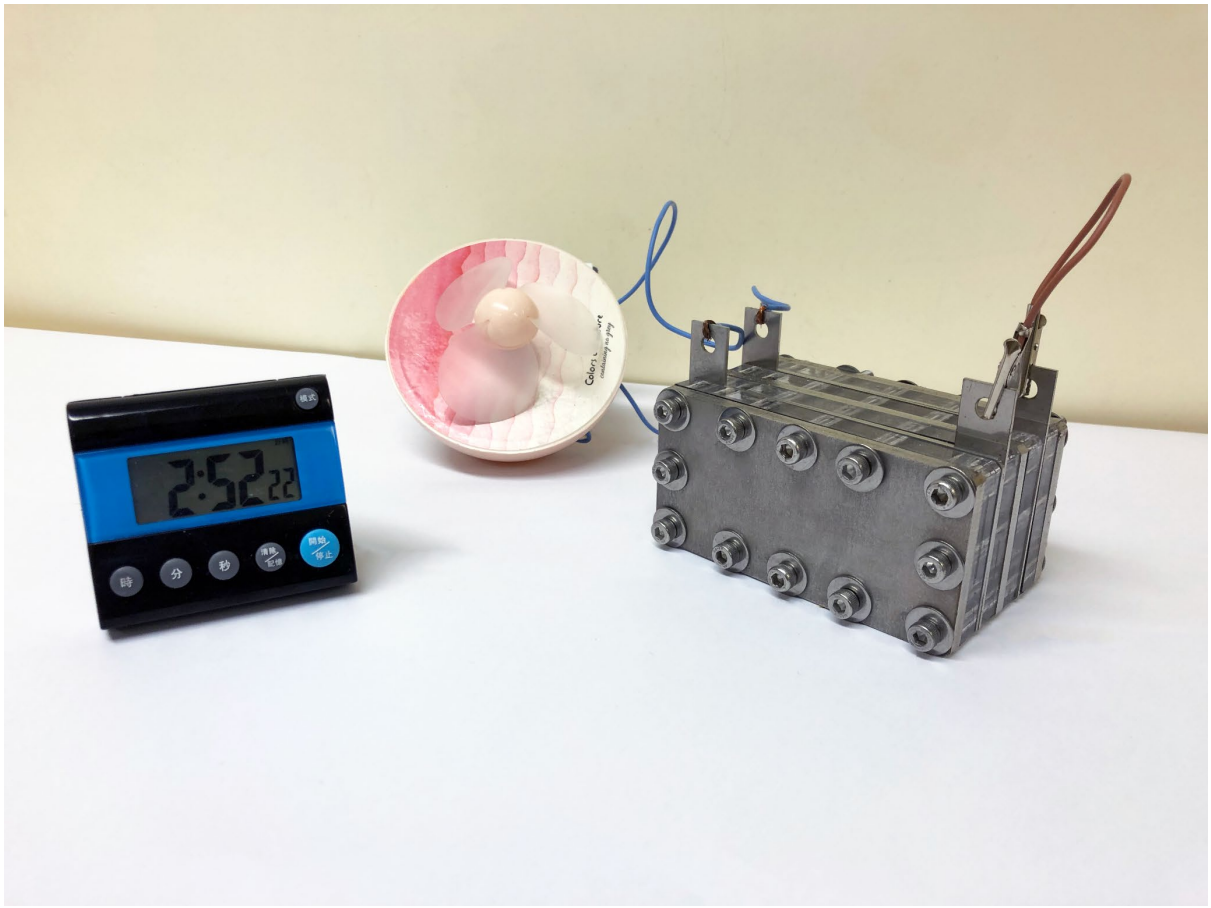

Fig. 8 (a) Running time of the fan powered by the passive stack under the ambient environment.

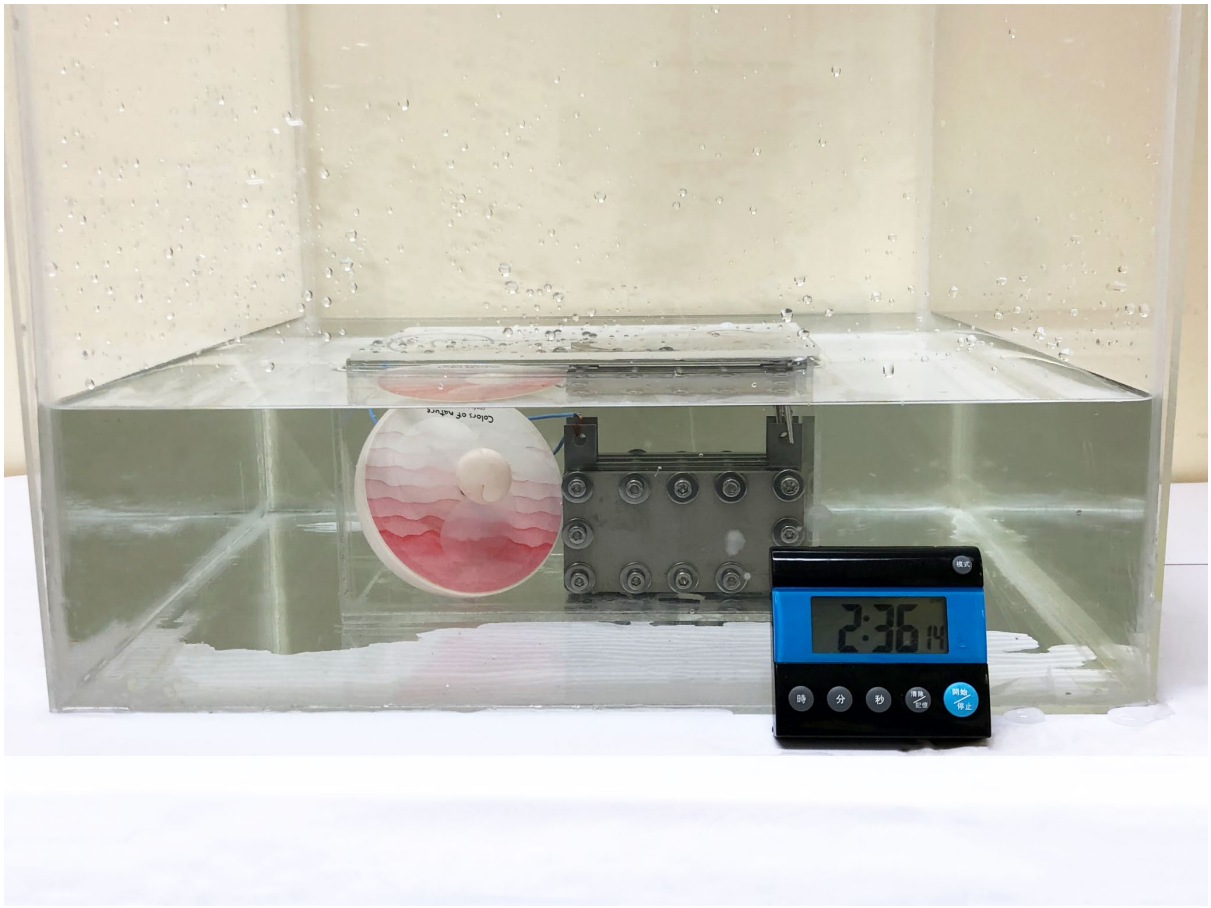

Fig. 8 (b) Running time of the fan powered by the passive stack under the imitated underwater environment.